energy&fuels

Article

pubs.acs.org/EF

Laminar Burning Velocities of C_4−C_7 Ethyl Esters in a Spherical Combustion Chamber: Experimental and Detailed Kinetic Modeling

Guillaume Dayma,*[,†,‡] Fabien Halter,[§] Fabrice Foucher,[§] Christine Mounaim-Rousselle,[§] and Philippe Dagaut[‡]

[†]Université d'Orléans, ICARE, UPR 3021, 1C avenue de la Recherche Scientifique, 45071 Orléans, France

[‡]Institut des Sciences de l'Ingénierie et des Systèmes (INSIS), Centre National de la Recherche Scientifique (CNRS), 1C Avenue de la Recherche Scientifique, 45071 Orléans, France

[§]PRISME, Université d'Orléans, Polytech Vinci, 45072 Orléans cedex 2, France

Supporting Information

ABSTRACT: To better understand the combustion characteristics of ethyl esters that could become second-generation biofuels, new experimental data were obtained for the combustion of a series of small ethyl esters. Unstretched laminar burning velocities of C_4−C_7 ethyl ester−air premixed laminar flames were measured in a spherical combustion chamber over a range of pressures (1−10 bar), initial temperatures (323−473 K), and equivalence ratios (0.7−1.5). These experiments were simulated as well as low-pressure flame structures, jet-stirred reactor species profiles, and ignition delays in shock tubes and rapid compression machines. A new detailed chemical kinetic reaction mechanism (1845 reactions versus 232 species) was developed and used in this work. The present model shows good agreement with the present experimental data and those taken from the literature. To interpret the results, sensitivity analyses were performed.

1. INTRODUCTION

The search for renewable fuels for ground and air transportation is growing because such chemicals could reduce net greenhouse gas emissions[1] and oil dependency. For ground transportation, ethanol is the most important fuel component in terms of volume production because it represents >90% of the production of biofuels worldwide.[2] However, the sustainability of ethanol as a fuel is frequently debated,[3−5] and other ex-biomass synthetic fuels have been proposed. Lignocelluloses could be used to produce more sustainable fuels,[6] including bioethanol, if the complexity and costs of production are reduced.[7] Ethyl esters obtained from the transesterification of triglycerides and bioethanol

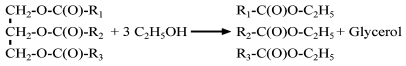

(1)

could become more attractive than methyl esters that derive from methanol, itself mostly produced from syngas. Furthermore, exhaust analyses conducted on rapeseed oil methyl and ethyl esters showed that the emissions of NO_x, CO, and smoke from the combustion of rapeseed oil ethyl ester were less harmful for the environment than that of rapeseed oil methyl ester.[8]

However, the database concerning the combustion of ethyl esters and their kinetics of oxidation is rather limited and needs new experimental and computational studies. Gasnot et al.[9,10] studied experimentally ethyl acetate (EA) oxidation in methane/oxygen/nitrogen low-pressure flames. Concentration profiles were obtained by microprobe sampling and gas chromatography (GC/TCD/FID and GC/MS) analyses. They observed that the addition of EA is responsible for an enhanced importance of C_2 and C_3 oxidation routes. A detailed chemical kinetic reaction mechanism was proposed to represent their experiments. In 2009, Walton et al.[11] studied the ignition of ethyl propionate (EP) in a rapid compression machine over a range of temperatures (935−1117 K), pressures (4.7−19.6 atm), and equivalence ratios (0.3−0.4). A chemical kinetic model was proposed to represent the data. In 2007, Metcalfe et al.[12] studied the ignition of EP in a high-temperature shock tube over a range of equivalence ratios (0.25−1.5), temperatures (1100−1670 K), and pressures (1.0 and 4.0 atm). Unimolecular decomposition produced propanoic acid and ethylene. This work was complemented later by jet-stirred reactor (JSR) experiments and modeling by Metcalfe et al.[13] The oxidation of EP was performed at 10 atm for equivalence ratios in the range of 0.3−2.0 and temperatures ranging from 750 to 1100 K. Concentration profiles of molecular species were used to propose a revised mechanism. They highlighted the importance of ethylene chemistry intermediately formed on the overall chemistry. Hakka et al.[14] published in 2010 an experimental and kinetic modeling study of the ignition of ethyl butanoate (EB) in a shock tube over a range of equivalence ratios (0.25−2) and temperatures (1250−2000 K) at a post-shock pressure of ∼8 atm. In 2010, Zhang and Boehman[15] studied the autoignition of ethyl hexanoate in a motored CFR engine at an equivalence ratio of 0.25 and an intake temperature of 428 K. GC−MS analyses indicated that the alkyl chain of ethyl hexanoate reacts via an alkane-like low-temperature oxidation sequence. Measurements of high level of C_2H_4 from ethyl hexanoate oxidation compared to methyl heptanoate indicated the existence

Received: July 26, 2012
Revised: September 14, 2012
Published: September 20, 2012

   dx.doi.org/10.1021/ef301254q | Energy Fuels 2012, 26, 6669−6677

Table 1. Experimental Data Used To Validate the Proposed Kinetic Mechanism

ester	experiment and data[a]	P (atm)	T (K)	X_{ester} (mol %)	φ	reference
EA	LPLF/SP	5.2×10^{-2}	400−1885	2	0.92	Gasnot et al.[10]
EA	LPLF/SP	3.95×10^{-2}	500−2330	17.12	1.58	Westbrook et al.[20]
EP	ST/ID	1/4	1165−1660	1/1.5	0.25/0.5/1/1.5	Metcalfe et al.[12]
EP	JSR/SP	10	770−1100	0.1	0.3/0.6/1/2	Metcalfe et al.[13]
EP	RCM/ID	10	990−1120	0.96/1.27	0.3/0.4	Walton et al.[11]
EP	LPLF/SP	3.95×10^{-2}	500−2110	13.97	1.56	Yang et al.[21]
EB	ST/ID	7.3−9.2	1280−1890	0.42/0.5/1	0.25/1/2	Hakka et al.[14]
EB	PFR/SP	1	500−1200	0.013	0.5−1.6	Bennadji et al.[16]

[a]ST, shock tube; RCM, rapid compression machine; JSR, jet-stirred reactor; LPLF, low-pressure laminar flame; PFR, plug-flow reactor; ID, ignition delay; and SP, species profiles.

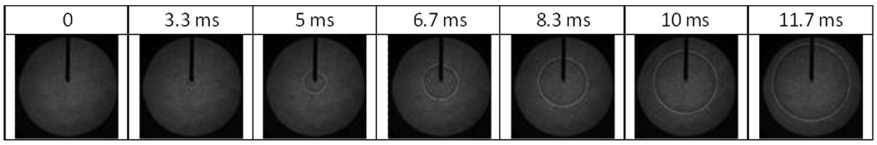

Figure 1. Shadowgraphs of the temporal evolution of the flame front for EP/air mixtures at P = 1 bar, T_u = 423 K, and φ = 0.9.

of ethylene molecular elimination during the low-temperature oxidation of ethyl esters. In 2011, Bennadji et al.[16] presented an experimental and kinetic modeling study of the oxidation of EB in a laminar atmospheric flow reactor over a range of temperatures (500−1200 K) and equivalence ratios (0.5−1.6). Concentration profiles were used to propose a detailed chemical kinetic reaction mechanism. Also in 2011, Akih-Kumgeh and Bergthorson[17] studied the high-temperature shock-tube ignition of EA and EP. They found that ethyl esters generally have shorter ignition delay times than corresponding methyl esters. They proposed a model to predict ignition delay times. The same year, Contino et al.[18] studied the combustion of EA, EP, and EB in a homogeneous charge compression ignition (HCCI) engine. They compared their results to ethanol taken as the reference fuel. They showed that ethanol ignites earlier. The same group also studied[19] the ignition timing for 12 different blends of ethyl esters (EA, EP, and ethyl butyrate). Low-pressure flat flame experiments have also been reported in the literature for EA[20] and EP.[21]

The aim of this study is 2-fold: (i) provide new experimental results for the combustion of ethyl esters by measuring burning velocities of premixed laminar flames over a range of equivalence ratios, temperatures, and pressures and (ii) propose a new detailed chemical kinetic reaction mechanism for the combustion of ethyl esters validated against the few experimental kinetic data available in the literature and gathered in Table 1.

Thanks to the use of different reactors, these data were obtained in a wide range of experimental conditions (pressure, temperature, and initial composition) allowing us to obtain a robust chemical kinetic mechanism.

2. EXPERIMENTAL SECTION

2.1. Laminar Flame Setup. The methodologies for fundamental flame speed determination include conical, flat, and counter-flow flames and outwardly spherically expanding flames.[22,23] In the rim-stabilized conical flame method, the premixed reactants flow toward the exit of a cylindrical tube, where a conical flame is anchored. The major drawback of this present configuration is that the burning velocity is not constant over the entire flame cone. Thus, the flame surface is not perfectly conical. It is also affected by heat losses at the burner rim. In the flat flame configuration, a flat flame is stabilized downstream of a water-cooled porous plate by adjusting the corresponding cooling water flow rate. The major drawback of the flat flame methodology is that the increase of the water-cooling temperature is rather small, which worsens the accuracy of the determined fundamental flame speeds. To circumvent this problem, the heat flux burner was developed. In this configuration, the flame is stabilized on a perforated brass plate. The latter is heated, warming up fresh gases flowing through the perforated brass plate. The counterflow flame methodology consists of impinging two identical laminar reactive jets onto each other. In this configuration, the flames are subjected to aerodynamic straining. In the spherically expanding flame method, the laminar flame is ignited at the center of the chamber and propagates in the outward direction. Similar to the counterflow flame method, an extrapolation is performed to yield the unstretched flame propagation speed, subsequently rescaled by the burnt/unburnt gas density ratio.

Here, the laminar flame burning velocity measurements were performed in the 4.2 L stainless-steel spherical combustion chamber used previously.[24−26] Four windows provided optical access into the chamber. Before filling the combustion chamber, it was pumped down to <1 mbar. Air was introduced into the chamber using a thermal mass flow controller. Synthetic air composed of 79.5% N_2 and 20.5% O_2 was used in the experiments. The liquid fuels (EA, CAS registry number 141−78−6; EP, CAS registry number 105−37−3; and EB, CAS registry number 105−54−4) were injected by means of a Coriolis mass flow meter (Bronkhorst, France). Injected air was directed to the exit of the Coriolis flow meters to convey the injected liquid. Before entering the chamber, the mixture was heated to 450 K to guarantee full vaporization of the fuel, which was checked via GC analyses.

The temperature of the chamber was regulated at the desired value in the range of 323−423 K. An electric fan was used to mix the reactants inside the chamber. Ignition was delayed to avoid any perturbation during the flame propagation experiments. Two tungsten electrodes separated by 1 mm and connected to a capacitive discharge ignition system were used to spark ignite the reactive mixture at the center of the chamber. Measurements were limited to flames with diameters <50 mm. This corresponds to a total volume of burnt gases <1.6% of the chamber volume. During the initial stage of the flame expansion, the total pressure inside the chamber can be considered constant. For every condition, the measurements were repeated 3 times. The standard deviation representing the scattering in experiments was ±2 cm/s.

Shadowgraphy flame images were recorded. Parallel light was obtained from an Ar ion laser source with two plano-convex lenses of 25 and 1000 mm focal lengths. The shadowgraphic images recorded

dx.doi.org/10.1021/ef301254q | Energy Fuels 2012, 26, 6669−6677

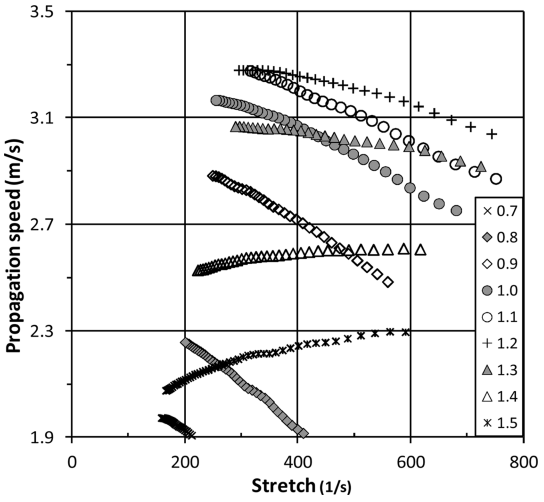

Figure 2. Evolution of the stretched propagation speed with stretch for the different EP/air mixtures at P = 1 bar and T_u = 423 K.

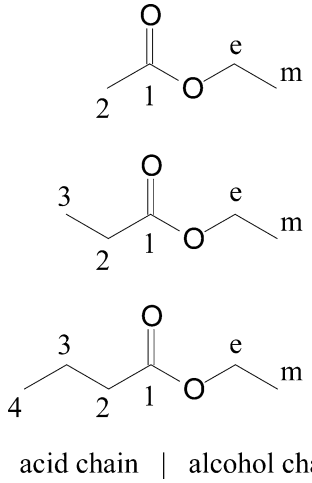

Figure 3. Ethyl ester structures with carbons labeled.

using a high-speed video camera (CMOS, Photron APX) were used to analyze the temporal evolution of the expanding spherical flames. It was operating at 10 000 frames/s with a 20 μs exposure time. After spark ignition, the flame front propagates spherically. This is illustrated in Figure 1 for an EP/air mixture at P = 1 bar, T_u = 423 K, and φ = 0.9.

2.2. Laminar Burning Velocity Extraction. The stretched spatial flame velocity was obtained from the variation of the flame radius (R_f) as a function of time (t).

$$S_b = \frac{dR_f}{dt} \tag{2}$$

For a spherical expanding laminar flame, the total stretch rate acting on the flame is defined as

$$k = 2\frac{S_b}{R_f} \tag{3}$$

The nonlinear relation between the propagation velocity and the stretch rate was used here to deduce the unstretched propagation speed (S_b^0)[27]

$$\left(\frac{S_b}{S_b^0}\right)^2 \ln\left(\frac{S_b}{S_b^0}\right)^2 = -\frac{2L_bK}{S_b^0} \tag{4}$$

where L_b is the burnt gas Markstein length. The use of this nonlinear formulation yields better results especially under fuel-lean conditions

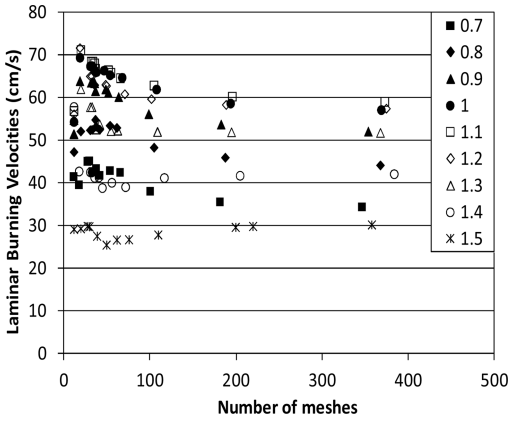

Figure 4. Evolution of the calculated laminar burning velocity with the number of meshes for different equivalence ratios of EA/air flames at T_u = 423 K and P = 1 bar.

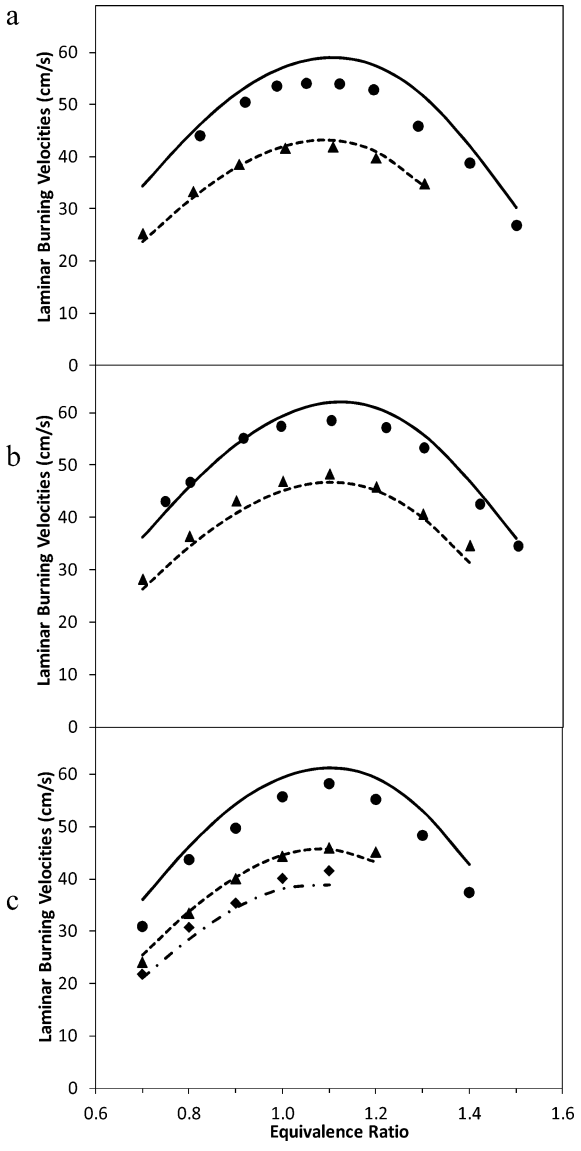

Figure 5. Experimental (symbols) and computed (lines) unstretched laminar burning velocities according to the equivalence ratio for (a) EA/air, (b) EP/air, and (c) EB/air flames at T_u = 423 K and P = 1 bar (● and —), P = 3 bar (▲ and - - -), and P = 5 bar (◆ and - · -).

dx.doi.org/10.1021/ef301254q | Energy Fuels 2012, 26, 6669–6677

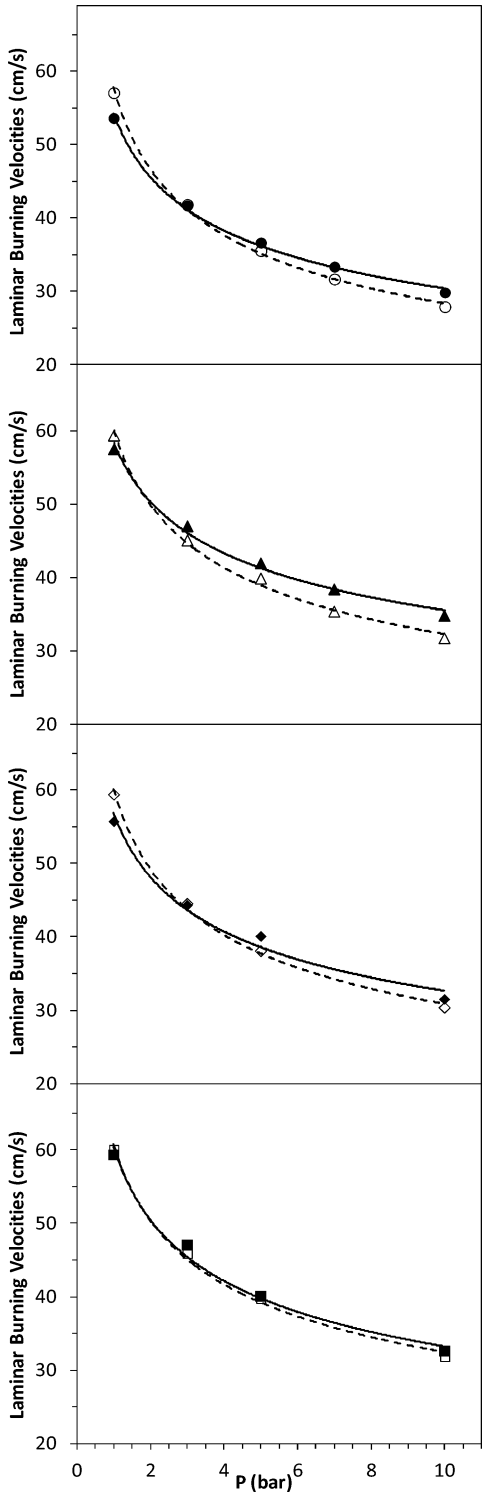

Figure 6. Experimental (filled symbols) and computed (open symbols) unstretched laminar burning velocities according to the initial pressure for EA/air (● and ○), EP/air (▲ and △), EB/air (◆ and ◇), and EPE/air (■ and □)[28] flames at T_u = 423 K (—, power regressions of experimental data; - - -, power regressions of computed data).

(i.e., when Markstein length values are far from unity). Propagation speeds for EP are presented in Figure 2 as a function of the stretch for the whole set of equivalence ratios studied. Up to an equivalence ratio of 1.2, the flame is accelerated when the stretch rate decreases (i.e., when the flame radius increases), corresponding to a positive burnt gas Markstein length.

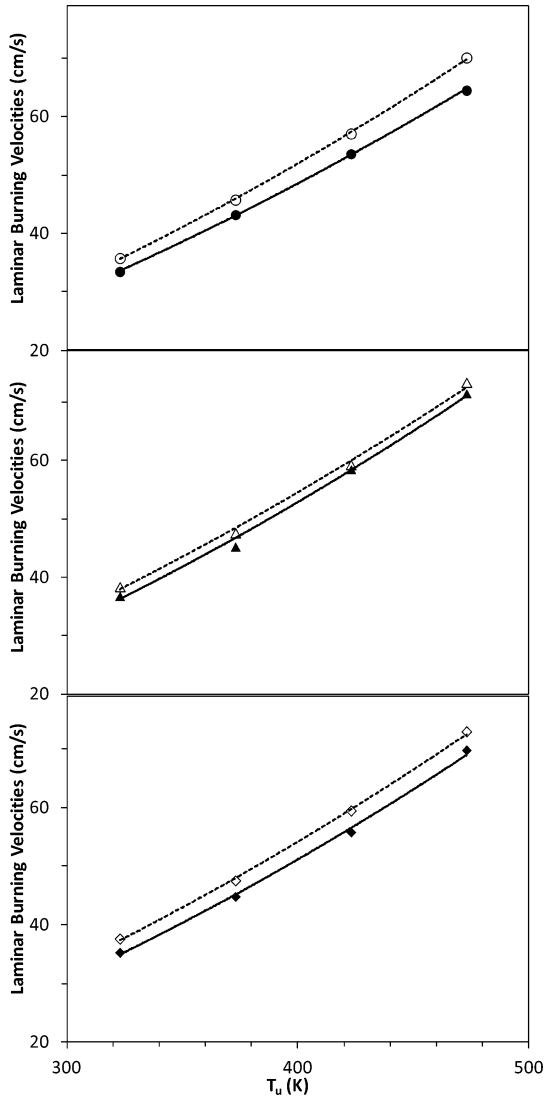

Figure 7. Experimental (filled symbols) and computed (open symbols) unstretched laminar burning velocities according to the temperature of the unburnt gases for EA/air (● and ○), EP/air (▲ and △), and EB/air (◆ and ◇) flames at P = 1 bar (—, power regressions of experimental data; - - -, power regressions of computed data).

Then, for constant pressure flame propagation, the laminar burning velocity can be derived from eq 5

$$S_u^0 = \frac{\rho_b}{\rho_u} S_b^0 \tag{5}$$

where ρ_b and ρ_u represent the density of burnt and unburnt gases, respectively. Details are given in the Appendix. The densities of the burnt gases were evaluated using the chemical composition at the constant pressure adiabatic conditions.

3. COMPUTATIONAL METHODS

The kinetic reaction mechanism used here was proposed to predict the oxidation of EPE at high temperatures.[28] This mechanism is the reduced version proposed in our previous work on EPE and was validated against JSR experimental data at a fixed residence time (0.7 s) and pressure (10 atm) over a range of equivalence ratios and temperatures and laminar burning velocities at different pressures and equivalence ratios. In this reduced version, the low-temperature chemistry (R + O_2 = RO_2 and subsequent reactions) was removed because low-temperature reactions are unimportant under the

dx.doi.org/10.1021/ef301254q | Energy Fuels 2012, 26, 6669–6677

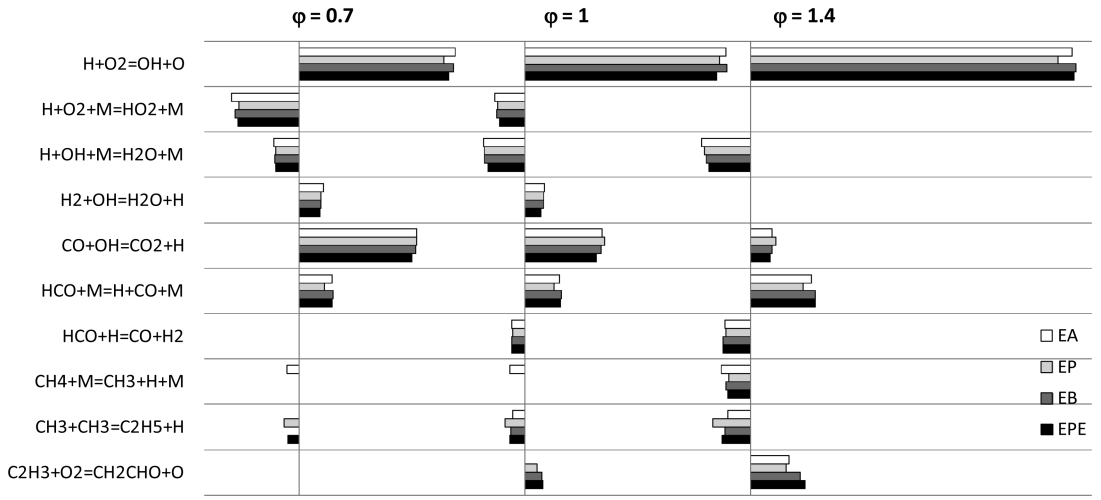

Figure 8. Ten most sensitive reactions regarding the flow rate for EA/air, EP/air, EB/air, and EPE/air flames at three different equivalence ratios (0.7, 1, and 1.4), T_u = 423 K, and P = 1 bar.

conditions of the present study. This also allows faster computations and easier reached numerical solutions. This detailed kinetic mechanism involves 1845 reactions and 232 species. For nomenclature consistency, carbon atoms of EA, EP, and EB were labeled as they were for EPE, with carbon number 1 being the carbon of the carbonyl group. These new studied ethyl ester structures with carbons labeled are presented in Figure 3.

Because the oxidation of EPE produces smaller radicals that can also be formed during the oxidation of EB, EP, or EA, the proposed detailed kinetic mechanism was also able to predict laminar burning velocities of ethyl esters from C_4 to C_7. Moreover, it was validated against various available experimental data on ethyl esters gathered in Table 1. The modeling of ethyl ester oxidation in the different experimental conditions was performed using the CHEMKIN package. JSR data were modeled using the PSR code.[29] Ignition delays in shock tubes or rapid compression machines were modeled using the SENKIN code.[30] Laminar flame burning velocities and burner-stabilized low-pressure flames species profiles were modeled using the PREMIX code.[31] The inputs for each simulation include a detailed chemical kinetic reaction mechanism, a data set of thermochemical properties, and a data set of transport properties. Mechanism, thermodynamic data, transport data, and laminar burning velocities for EA, EP, and EB are available in the Supporting Information and from the authors.

To summarize briefly, the reactions considered in the proposed mechanism were the same as for EPE and the rate constants used were estimated following the same structure−reactivity relationships. For instance, the molecular elimination of ethylene, also yielding alkanoic acids, were the same for all ethyl esters. Hydrogen abstractions by small radicals were also taken from our previous studies on methyl esters[32−34] for carbon atoms on the acid chain and carbon "m" (see Figure 3), and from our work on isopentanol[35] for carbon "e", as we did in the EPE submechanism.[28]

Finally, all of the laminar burning velocities were calculated with the same conditions of gradient and curvature (GRAD = 0.05 and CURV = 0.05), leading to a similar number of meshes for each equivalence ratio between 327 and 399. These conditions allow for the calculated laminar burning velocity to vary less than 2.5% between the two last calculation steps, as shown in Figure 4 in the case of different equivalence ratios of EA/air flames at T_u = 423 K and P = 1 bar.

4. RESULTS AND DISCUSSION

4.1. Laminar Flame Burning Velocities. The proposed model was used to predict unstretched laminar burning velocities of EA, EP, and EB. The laminar burning velocities were

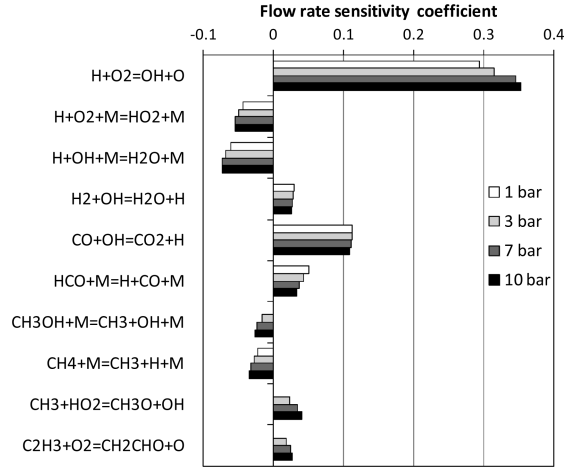

Figure 9. Ten most sensitive reactions regarding the flow rate for stoichiometric EA/air flames according to the pressure at T_u = 423 K.

determined over a range of equivalence ratios (0.7−1.5) at several pressures and different unburnt gas temperatures.

Figure 5 compares the experimental and simulated laminar burning velocities according to the equivalence ratio, at different pressures for (a) EA, (b) EP, and (c) EB. The ±2 cm/s experimental standard deviation is contained in the symbol size.

For the three ethyl esters studied, the experimental data obtained indicate that the burning velocity increases between φ = 0.7 and 1.1, at which a maximum burning velocity was observed at every pressure, and then decreases at higher equivalence ratios. Moreover, the maximum burning velocity is very close for each ethyl ester (at 1 bar, 54.1 cm/s for EA, 58.6 cm/s for EP, 58.2 cm/s for EB, and 59.3 cm/s for EPE[28]), with EA laminar burning velocities being the lowest regardless of the pressure. The model well predicts the change in laminar burning velocity as the equivalence ratio is increased from 0.7 to 1.5. At φ = 1.1 and P = 1 bar, the maximum burning velocity predicted by the model is 59.0 cm/s for EA, 61.95 cm/s for EP, 61.25 cm/s for EB, and 61.49 cm/s for EPE, corresponding to a difference with the experimental data <10% in all cases. At 3 bar, the agreement between calculations and experimental data goes under 3% at φ = 1.1. This better agreement at higher pressure can be related to a slightly distorted estimation of the

dx.doi.org/10.1021/ef301254q | Energy Fuels 2012, 26, 6669−6677

laminar burning velocity at P = 1 bar because of the use of the density ratio, as explained elsewhere.[36]

Figure 6 presents the effect of the pressure on burning velocities of ethyl ester/air stoichiometric mixtures. Filled symbols are the experimental values at different pressures, and open symbols are the modeling results obtained with the proposed kinetic reaction mechanism. Our model slightly overpredicts the laminar burning velocities for the three studied ethyl esters at 1 bar and slightly underpredicts the laminar burning velocities for the three studied ethyl esters at the highest pressures. Nevertheless, the developed kinetic model is able to predict the flame laminar burning velocities of such mixtures all over the pressure range, taking into account the experimental and numerical errors. According to our results, laminar burning velocities of ethyl ester/air mixtures present negative-pressure dependencies of $P^{-0.251}$ for EA, $P^{-0.215}$ for EP, and $P^{-0.241}$ for EB at φ = 1 and T = 423 K, which is similar to what was obtained in our previous study with EPE.[25]

Figure 7 presents the effect of the initial temperature on burning velocities of ethyl ester/air stoichiometric mixtures. Filled symbols are the experimental values at different temperatures of fresh gases, and open symbols are the modeling results obtained with the proposed kinetic reaction mechanism. Our model slightly overpredicts the laminar burning velocities (+5.6 cm/s in the worst case, i.e., EA at 473 K) for the three studied ethyl esters all over the temperature range, but the slope of the temperature dependence is well-captured. According to our results, laminar burning velocities of ethyl ester/air mixtures present positive-temperature dependencies of $T^{1.72}$ for EA, $T^{1.76}$ for EP, and $T^{1.78}$ for EB at φ = 1 and P = 1 bar.

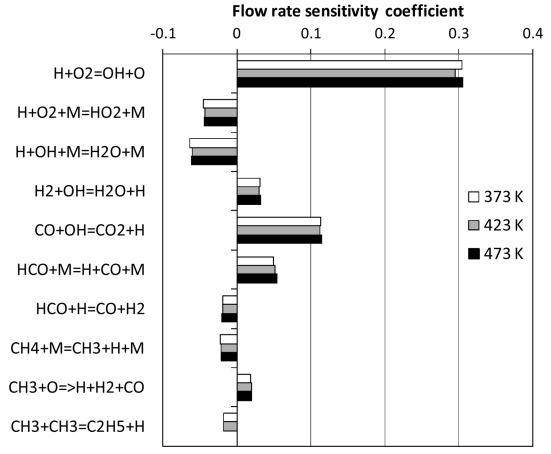

Figure 10. Ten most sensitive reactions regarding the flow rate for stoichiometric EA/air flames according to the initial temperature at P = 1 bar.

4.2. Sensitivity Analyses on Laminar Flame Burning Velocities. Sensitivity analyses on burning velocity were performed at different equivalence ratios, pressures, and initial temperatures to determine which reactions are sensitive to which fuel. Figure 8 shows the 10 most sensitive reactions regarding the flow rate for EA, EP, EB, and EPE at three equivalence ratios, φ = 0.7, 1, and 1.4. For clarity purposes, the labels of the x axis have been removed but the scale was kept constant for the three equivalence ratios. The first observation is that, for one equivalence ratio, the sensitivity coefficients are very similar for the same reaction regardless of the ester. Moreover, the most sensitive reaction, regardless of the equivalence ratio and the ester, is the branching reaction, $H + O_2 \rightleftharpoons OH + O$, which accelerates the flame. The sensitivity of this reaction increases with the equivalence ratio. Under lean conditions, this reaction competes with $H + O_2 + M \rightleftharpoons HO_2 + M$. The sensitivity of this reaction decreases when the equivalence ratio increases. Another sensitive reaction is the oxidation of CO by OH, yielding CO_2 and H atoms. The accelerating effect of this reaction is mostly sensitive under lean conditions. When the equivalence ratio increases, the amount of hydroxyl radicals decreases as well as the sensitivity of this reaction.

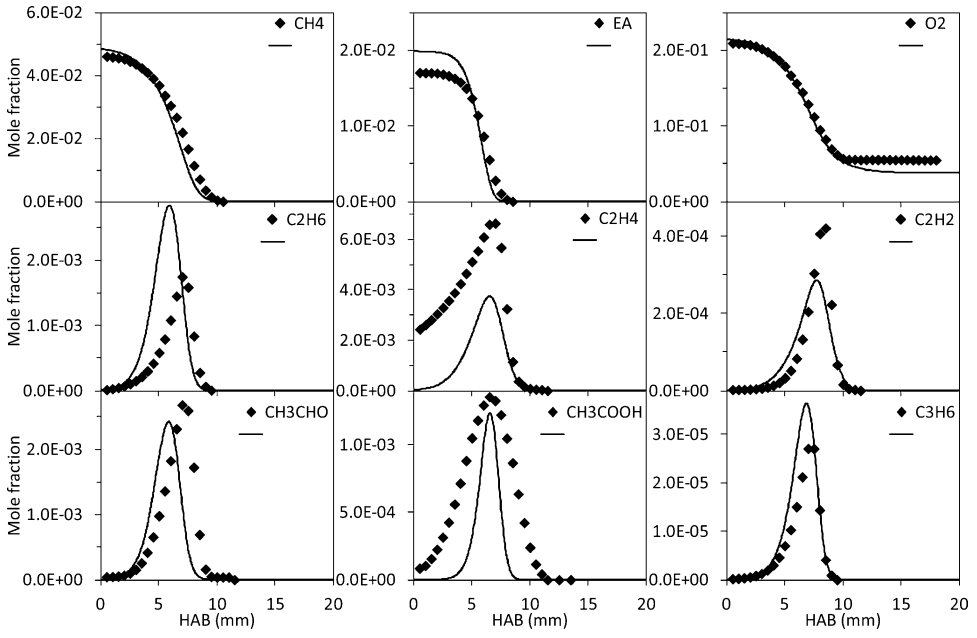

Figure 11. Mole fractions of reactants and intermediates according height above the burner for a CH_4/2% EA/O_2/N_2 flame at P = 5263 Pa. Symbols are experimental data,[9] and lines are calculation results.

dx.doi.org/10.1021/ef301254q | Energy Fuels 2012, 26, 6669–6677

Water formation by recombination of H and OH slows the flame with a sensitivity slightly increasing with the equivalence ratio and the sensitivity of the decomposition of formyl radicals (HCO) in H and CO, which accelerates the flame, slightly increasing with the equivalence ratio. Furthermore, with the increase of the equivalence ratio, the flame speed becomes sensitive to methyl recombination reactions (with H or CH_3 itself) and the reaction of vinyl radicals with O_2, yielding CH_2CHO and O atoms. Finally, no reaction involving the fuels is sensitive regarding the flame speed regardless of the equivalence ratio.

Sensitivity analyses were also performed on the flow rate according to the pressure for stoichiometric EA/air flames at T_u = 423 K. These results are presented in Figure 9. The computed burning velocity is mostly sensitive to reactions involving small species. Regardless of the pressure, no reaction involving the fuel is sensitive regarding the flame speed. Among them, one finds the main branching reaction, $H + O_2 \rightleftharpoons OH + O$, which is the most sensitive and in which sensitivity increases with the pressure. Moreover, the sensitivity of recombination reactions increases with the pressure ($H + O_2 + M \rightleftharpoons HO_2 + M$, $H + OH + M \rightleftharpoons H_2O + M$, $CH_3 + OH + M \rightleftharpoons CH_3OH + M$, and $CH_4 + M \rightleftharpoons CH_3 + H + M$), whereas the sensitivity of dissociation reactions decreases when the pressure increases ($HCO + M \rightleftharpoons H + CO + M$).

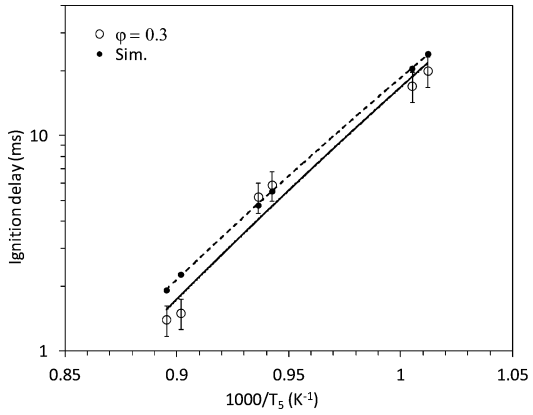

Figure 12. Ignition delays of $EP/O_2/N_2/Ar$ mixtures at φ = 0.3 and P = 10 atm in a rapid compression machine. Empty symbols are experimental data,[11] and filled symbols are calculation results. Lines are regressions.

Finally, sensitivity analyses on the flow rate according to the temperature of fresh gases were performed in the case of stoichiometric EA/air flames at P = 1 bar. These results are presented in Figure 10. Again, over 100 °C, no reaction involving the fuel is sensitive regarding the flame speed regardless of the the initial temperature. Moreover, for the 10 most sensitive reactions, the sensitivity coefficients are equivalent for the same reaction regardless of the initial temperature. Under these conditions, the reactions for which an increase of the rate constant increases the flame burning velocities are $H + O_2 \rightleftharpoons OH + O$, $CO + OH \rightleftharpoons CO_2 + H$, $HCO + M \rightleftharpoons H + CO + M$, and $H_2 + OH \rightleftharpoons H_2O + H$. Conversely, recombination reactions, e.g., $H + O_2 + M \rightleftharpoons HO_2 + M$, $H + OH + M \rightleftharpoons H_2O + M$, and $CH_4 + M \rightleftharpoons CH_3 + H + M$, would reduce burning velocities if their rate was increased.

4.3. Other Experimental Devices. Our detailed kinetic mechanism was tested on experimental data from the literature. As presented in Table 1, Gasnot et al.[9] studied methane/air low-pressure laminar flames seeded with different amounts of EA. Mole fraction profiles of several species were measured. As seen Figure 11, the case of a flame doped with 2% EA, our kinetic scheme reproduces well the consumption of the reactants and most of the intermediate. The presently proposed scheme underestimates the acetic acid peak concentration, while the study by Gasnot et al.[10] overestimates the acetic acid peak concentration. This is due to the different kinetic parameters used for the molecular elimination yielding acetic acid. An uncertainty remains regarding the initial amount of EA. In the burner, EA might have been converted into ethylene and acetic acid. The missing 0.3% EA matches well with the 0.25% ethylene at the burner. Figure 12 shows the evolution of the ignition delay of $EP/O_2/N_2/Ar$ mixtures in a rapid compression machine at φ = 0.3 and P = 10 atm. These delays are between 1.4 and 20 ms for a temperature range between 988 and 1117 K, and our calculations are in good agreement with these experimental data from Walton et al.[11] Figure 13 depicts how our detailed kinetic mechanism performs against the

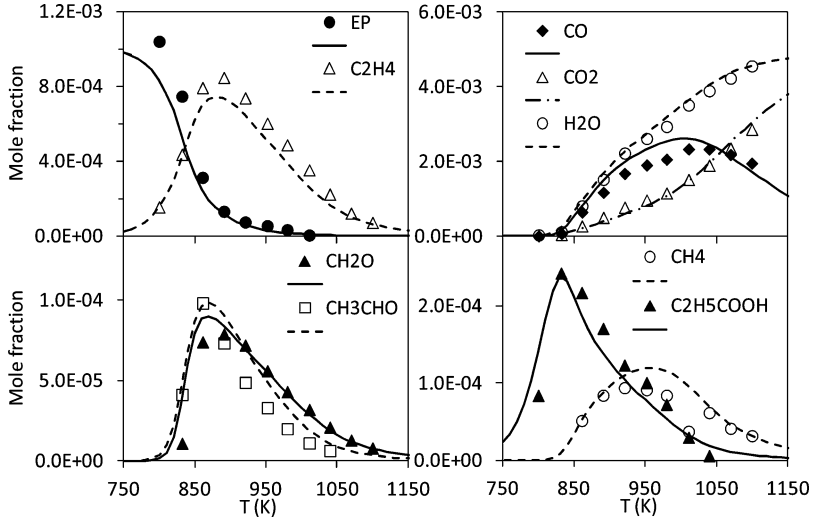

Figure 13. Mole fractions of reactants, intermediates, and final products in a JSR at P = 10 bar, φ = 1, and τ = 0.7 s. Symbols are experimental data,[13] and lines are calculation results.

dx.doi.org/10.1021/ef301254q | Energy Fuels 2012, 26, 6669−6677

oxidation of EP in a JSR. This figure shows the evolution of the mole fractions of EP, ethylene, CO, CO_2, H_2O, formaldehyde, acetaldehyde, methane, and propanoic acid at P = 10 atm, φ = 1, and a residence time, τ = 0.7 s. Our kinetic mechanism reproduces very well the conversion of the fuel as well as the formation of intermediates and final products presented by Metcalfe et al.[13] Finally, Figure 14 compares the experimental

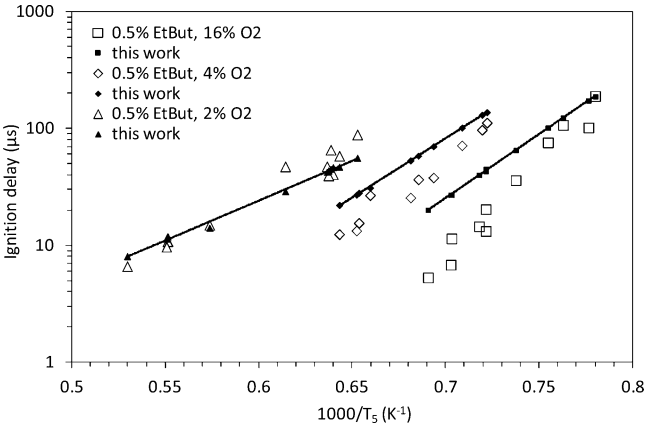

Figure 14. Ignition delays of EB/O_2/Ar mixtures at P = 8 bar and φ = 0.25 (□), φ = 1 (◇), and φ = 2 (△) in a shock tube. EtBut stands for EB. Empty symbols are experimental data,[14] and filled symbols are calculation results. Lines are regressions.

ignition delays measured by Hakka et al.[14] in a shock tube for EB at three different equivalence ratios and our calculations using our detailed kinetic mechanism. The global activation energy is well-reproduced, and the agreement is globally satisfactory even if high-temperature ignition delays of the lean mixture are overestimated by our model.

5. CONCLUSION

New laminar burning velocities were obtained for ethyl esters in a spherical combustion chamber. The effect of the pressure on the laminar burning velocity was investigated. Laminar flame burning velocities were measured at 1, 3, 5, and 10 bar. The data showed that burning velocity varies as a function of $P^{-0.251}$ for EA, $P^{-0.215}$ for EP, and $P^{-0.241}$ for EB at φ = 1 and T = 423 K. The laminar burning velocities of ethyl esters as well as species profiles in a flat flame and JSR and ignition delays in a shock tube and rapid compression machine were modeled with the help of a detailed chemical kinetic reaction mechanism (1845 reactions involving 232 species). The kinetic modeling obtained thanks to the proposed detailed kinetic reaction mechanism agrees well with the present laminar burning velocities obtained in a spherical combustion chamber. Sensitivity analyses on the flame speed were conducted according to the chain length of the fuel, the pressure, and the initial temperature. It appears that the laminar burning velocity is mostly sensitive to the chemistry of small species. The proposed kinetic reaction mechanism could now be extended to larger ethyl esters more suitable for diesel application.

APPENDIX

In the following, it is assumed that the flame remains smooth and spherical. There are no pressure gradients within the vessel. If chemistry is rapid enough, one can only consider unburnt and burnt gases.

Mass conservation gives

$$m_0 = m_u + m_b \tag{A1}$$

$$\frac{dm_u}{dt} = -\frac{dm_b}{dt} \tag{A2}$$

where subscripts 0, u, and b indicate initial reference, unburnt gas, and burnt gas states, respectively.

In a spherical geometry, the rate of burning is expressed as the rate of consumption of reactants at an initial unburnt gas density ρ_u and radius r_u, with an associated burning velocity S_u.

$$\frac{dm_u}{dt} = -4\pi {r_u}^2 \rho_u S_u \tag{A3}$$

r_u is the radial distance to the boundary of the unburnt gas of density ρ_u. In practical application, the flame radius do not exactly correspond to r_u, because of the rate of change of the flame thickness with the radius.

The burning rate is also expressed as the rate of consumption of fresh gases

$$\frac{dm_u}{dt} = -\frac{d}{dt}\left(\int_0^{r_u} \rho_b 4\pi r^2 dr\right) \tag{A4}$$

with ρ_b being the burnt gas density.

Identifying the two previous equations, one can obtained an expression of the stretched laminar burning velocity.

$$S_u = \frac{1}{r_u^2 \rho_u} \times \frac{d}{dt}\left(\int_0^{r_u} \rho_b r^2 dr\right) \tag{A5}$$

A mean density, $\overline{\rho}_b$, is defined for the gas within the radius r_u as $\overline{\rho}_b = (\int_0^{r_u} 4\pi r^2 \rho dr)/(\int_0^{r_u} 4\pi r^2 dr)$. We make the assumption of a global isentropic compression law for burnt gases. In these conditions, eq A5 may be simplified to

$$S_u = \frac{\overline{\rho}_b}{\rho_u}\frac{dr_u}{dt} + \frac{r_u}{3\rho_u}\frac{d\overline{\rho}_b}{dt} = \frac{\overline{\rho}_b}{\rho_u}\frac{dr_u}{dt} + \frac{r_u \overline{\rho}_b}{3\gamma_b \rho_u P}\frac{dP}{dt} \tag{A6}$$

This equation was previously expressed by Bradley and Mitcheson.[37]

Usually, the visualization process is limited to relatively low flame reduced diameters (flame diameter adimensionned by the vessel diameter). In these conditions, the compression effect is limited. In these conditions, the stretched laminar burning velocity may be evaluated using the expression

$$S_u = \frac{\overline{\rho}_b}{\rho_u}\frac{dr_u}{dt} = \frac{\overline{\rho}_b}{\rho_u} S_b \tag{A7}$$

where S_b is the propagation speed of the flame front.

ASSOCIATED CONTENT

Supporting Information

Proposed chemical kinetic reaction mechanism in CHEMKIN format, associated thermochemical and transport data in CHEMKIN format, and experimental data. This material is available free of charge via the Internet at http://pubs.acs.org.

AUTHOR INFORMATION

Corresponding Author

*Telephone: (+33) 238-255499. Fax: (+33) 238-696004. E-mail: guillaume.dayma@cnrs-orleans.fr.

Notes

The authors declare no competing financial interest.

■ ACKNOWLEDGMENTS

The research leading to these results has received funding from the European Research Council under the European Community's Seventh Framework Programme (FP7/2007-2013)/ERC Grant Agreement 291049-2G-CSafe.

■ REFERENCES

(1) Demirbas, A. Progress and recent trends in biofuels. *Prog. Energy Combust. Sci.* **2007**, *33* (1), 1−18.
(2) Energy Information Administration (EIA). *International Energy Outlook 2006*; EIA, Office of Integrated Analysis and Forecasting, U.S. Department of Energy: Washington, D.C., June 2006.
(3) Jacobson, M. Z. Effects of ethanol (E85) versus gasoline vehicles on cancer and mortality in the United States. *Environ. Sci. Technol.* **2007**, *41* (11), 4150−4157.
(4) Elcock, D. Projected water consumption for ethanol and biodiesel production relative to other sectors in 2030. *Abstr. Pap. Am. Chem. Soc.* **2009**, 238.
(5) Elcock, D. Future US water consumption: The role of energy production. *J. Am. Water Resour. Assoc.* **2010**, *46* (3), 447−460.
(6) Cheng, J. J.; Timilsina, G. R. Status and barriers of advanced biofuel technologies: A review. *Renewable Energy* **2011**, *36* (12), 3541−3549.
(7) Lange, J.-P.; Price, R.; Ayoub, P. M.; Louis, J.; Petrus, L.; Clarke, L.; Gosselink, H. Valeric biofuels: A platform of cellulosic transportation fuels. *Angew. Chem., Int. Ed.* **2010**, *49* (26), 4479−4483.
(8) Makareviciene, V.; Janulis, P. Environmental effect of rapeseed oil ethyl ester. *Renewable Energy* **2003**, *28* (15), 2395−2403.
(9) Gasnot, L.; Decottignies, V.; Pauwels, J. F. Ethyl acetate oxidation in flame condition: An experimental study. *Fuel* **2004**, *83* (4−5), 463−470.
(10) Gasnot, L.; Decottignies, V.; Pauwels, J. F. Kinetics modelling of ethyl acetate oxidation in flame conditions. *Fuel* **2005**, *84* (5), 505−518.
(11) Walton, S. M.; Wooldridge, M. S.; Westbrook, C. K. An experimental investigation of structural effects on the auto-ignition properties of two C5 esters. *Proc. Combust. Inst.* **2009**, *32* (1), 255−262.
(12) Metcalfe, W. K.; Dooley, S.; Curran, H. J.; Simmie, J. M.; El-Nahas, A. M.; Navarro, M. V. Experimental and modeling study of $C_5H_{10}O_2$ ethyl and methyl esters. *J. Phys. Chem. A* **2007**, *111* (19), 4001−4014.
(13) Metcalfe, W. K.; Togbe, C.; Dagaut, P.; Curran, H. J.; Simmie, J. M. A jet-stirred reactor and kinetic modeling study of ethyl propanoate oxidation. *Combust. Flame* **2009**, *156* (1), 250−260.
(14) Hakka, M. H.; Bennadji, H.; Biet, J.; Yahyaoui, M.; Sirjean, B.; Warth, V.; Coniglio, L.; Herbinet, O.; Glaude, P. A.; Billaud, F.; Battin-Leclerc, F. Oxidation of methyl and ethyl butanoates. *Int. J. Chem. Kinet.* **2010**, *42* (4), 226−252.
(15) Zhang, Y.; Boehman, A. L. Experimental study of the autoignition of $C_8H_{16}O_2$ ethyl and methyl esters in a motored engine. *Combust. Flame* **2010**, *157* (3), 546−555.
(16) Bennadji, H.; Glaude, P. A.; Coniglio, L.; Billaud, F. Experimental and kinetic modeling study of ethyl butanoate oxidation in a laminar tubular plug flow reactor. *Fuel* **2011**, *90* (11), 3237−3253.
(17) Akih-Kumgeh, B.; Bergthorson, J. M. Experimental and modeling study of trends in the high-temperature ignition of methyl and ethyl esters. *Energy Fuels* **2011**, *25* (10), 4345−4356.
(18) Contino, F.; Foucher, F.; Mounaim-Rousselle, C.; Jeanmart, H. Experimental characterization of ethyl acetate, ethyl propionate, and ethyl butanoate in a homogeneous charge compression ignition engine. *Energy Fuels* **2011**, *25* (3), 998−1003.
(19) Contino, F.; Foucher, F.; Mounaim-Rousselle, C.; Jeanmart, H. Combustion characteristics of tricomponent fuel blends of ethyl acetate, ethyl propionate, and ethyl butyrate in homogeneous charge compression ignition (HCCI). *Energy Fuels* **2011**, *25* (4), 1497−1503.
(20) Westbrook, C. K.; Pitz, W. J.; Westmoreland, P. R.; Dryer, F. L.; Chaos, M.; Osswald, P.; Kohse-Höinghaus, K.; Cool, T. A.; Wang, J.; Yang, B.; Hansen, N.; Kasper, T. A detailed chemical kinetic reaction mechanism for oxidation of four small alkyl esters in laminar premixed flames. *Proc. Combust. Inst.* **2009**, *32* (1), 221−228.
(21) Yang, B.; Westbrook, C. K.; Cool, T. A.; Hansen, N.; Kohse-Hoinghaus, K. Fuel-specific influences on the composition of reaction intermediates in premixed flames of three $C_5H_{10}O_2$ ester isomers. *Phys. Chem. Chem. Phys.* **2011**, *13* (15), 7205−7217.
(22) Law, C. K. *Combustion Physics*, 1st ed.; Cambridge University Press: New York, 2006; p 738.
(23) Bouvet, N. Experimental and numerical studies of the fundamental flame speeds of methane/air and syngas (H_2/CO)/air mixtures. Thesis, University of Orléans, Orléans, France, 2009; http://tel.archives-ouvertes.fr/tel-00473266/fr/.
(24) Sarathy, S. M.; Thomson, M. J.; Togbe, C.; Dagaut, P.; Halter, F.; Mounaim-Rousselle, C. An experimental and kinetic modeling study of *n*-butanol combustion. *Combust. Flame* **2009**, *156* (4), 852−864.
(25) Galmiche, B.; Togbe, C.; Dagaut, P.; Halter, F.; Foucher, F. Experimental and detailed kinetic modeling study of the oxidation of 1-propanol in a pressurized jet-stirred reactor (JSR) and a combustion bomb. *Energy Fuels* **2011**, *25* (5), 2013−2021.
(26) Togbé, C.; Dagaut, P.; Mzé-Ahmed, A.; Diévart, P.; Halter, F.; Foucher, F. Experimental and detailed kinetic modeling study of 1-hexanol oxidation in a pressurized jet-stirred reactor (JSR) and a combustion bomb. *Energy Fuels* **2010**, *24* (11), 5859−5875.
(27) Halter, F.; Tahtouh, T.; Mounaïm-Rousselle, C. Nonlinear effects of stretch on the flame front propagation. *Combust. Flame* **2010**, *157* (10), 1825−1832.
(28) Dayma, G.; Halter, F.; Foucher, F.; Togbé, C.; Mounaim-Rousselle, C.; Dagaut, P. Experimental and detailed kinetic modeling study of ethyl pentanoate (ethyl valerate) oxidation in a jet stirred reactor and laminar burning velocities in a spherical combustion chamber. *Energy Fuels* **2012**.
(29) Glarborg, P.; Kee, R. J.; Grcar, J. F.; Miller, J. A. *PSR: A FORTRAN Program for Modeling Well-Stirred Reactors*; Sandia National Laboratories: Livermore, CA, 1986; SAND86-8209.
(30) Lutz, A. E.; Kee, R. J.; Miller, J. A. *Senkin: A Fortran Program for Predicting Homogeneous Gas Phase Chemical Kinetics with Sensitivity Analysis*; Sandia National Laboratories: Livermore, CA, 1987.
(31) Kee, R. J.; Grcar, J. F.; Smooke, M. D.; Miller, J. A. *A Fortran Program for Modeling Steady Laminar One-Dimensional Premixed Flames*; Sandia National Laboratories: Livermore, CA, 1985; SAND85-8240.
(32) Dayma, G.; Gail, S.; Dagaut, P. Experimental and kinetic modeling study of the oxidation of methyl hexanoate. *Energy Fuels* **2008**, *22* (3), 1469−1479.
(33) Dayma, G.; Togbé, C.; Dagaut, P. Detailed kinetic mechanism for the oxidation of vegetable oil methyl esters: New evidence from methyl heptanoate. *Energy Fuels* **2009**, *23* (9), 4254−4268.
(34) Dayma, G.; Sarathy, S. M.; Togbé, C.; Yeung, C.; Thomson, M. J.; Dagaut, P. Experimental and kinetic modeling of methyl octanoate oxidation in an opposed-flow diffusion flame and a jet-stirred reactor. *Proc. Combust. Inst.* **2011**, *33* (1), 1037−1043.
(35) Dayma, G.; Togbe, C.; Dagaut, P. Experimental and detailed kinetic modeling study of isoamyl alcohol (isopentanol) oxidation in a jet-stirred reactor at elevated pressure. *Energy Fuels* **2011**, *25* (11), 4986−4998.
(36) Varea, E.; Modica, V.; Vandel, A.; Renou, B. Measurement of laminar burning velocity and Markstein length relative to fresh gases using a new postprocessing procedure: Application to laminar spherical flames for methane, ethanol and isooctane/air mixtures. *Combust. Flame* **2012**, *159* (2), 577−590.
(37) Bradley, D.; Mitcheson, A. Mathematical solutions for explosions in spherical vessels. *Combust. Flame* **1976**, *26*, 201−217.